INORGANIC CHEMISTRY
FRONTIERS

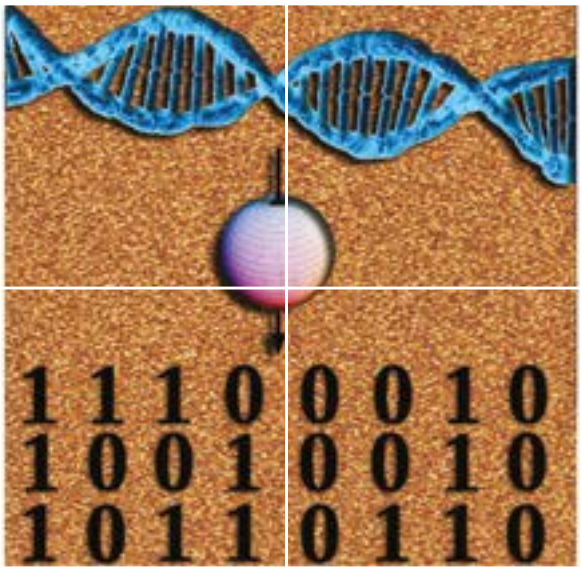

Accepted Manuscript

This article can be cited before page numbers have been issued, to do this please use: C. Wang, D. Sun, X. Yu, X. Zhang, Z. Lu, X. Wang, J. L. Zhao, L. Li and X. Yang, *Inorg. Chem. Front.*, 2018, DOI: 10.1039/C8QI00492G.

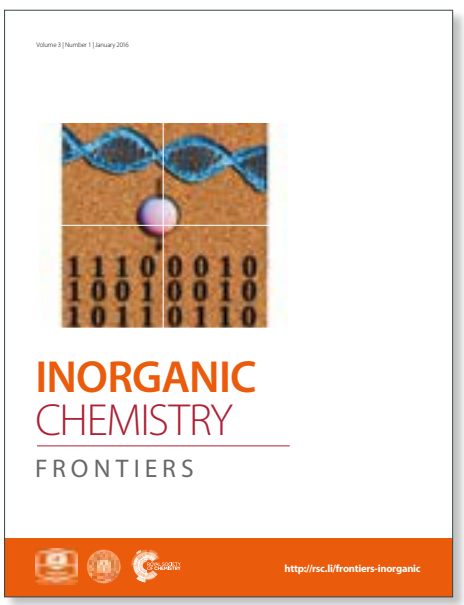

This is an Accepted Manuscript, which has been through the Royal Society of Chemistry peer review process and has been accepted for publication.

Accepted Manuscripts are published online shortly after acceptance, before technical editing, formatting and proof reading. Using this free service, authors can make their results available to the community, in citable form, before we publish the edited article. We will replace this Accepted Manuscript with the edited and formatted Advance Article as soon as it is available.

You can find more information about Accepted Manuscripts in the author guidelines.

Please note that technical editing may introduce minor changes to the text and/or graphics, which may alter content. The journal's standard Terms & Conditions and the ethical guidelines, outlined in our author and reviewer resource centre, still apply. In no event shall the Royal Society of Chemistry be held responsible for any errors or omissions in this Accepted Manuscript or any consequences arising from the use of any information it contains.

View Article Online
DOI: 10.1039/C8QI00492G

Journal Name

ARTICLE

Cu/Ni nanoparticles supported on TiO_2(B) nanotubes as hydrogen generation photocatalysts via hydrolysis of ammonia borane

Received 00th January 20xx,
Accepted 00th January 20xx

DOI: 10.1039/x0xx00000x

www.rsc.org/

Chenyang Wang[a], Dongdong Sun[a], Xiaofei Yu[a], Xinghua Zhang[a], Zunming Lu[a], Xixin Wang, Jianling Zhao[a]*, Lanlan Li[a]*, Xiaojing Yang [a]*

TiO_2(B) nanotubes (NTs) were used as carriers to support metal Cu/Ni nanoparticles for the catalytic hydrolysis of ammonia borane (NH_3BH_3, AB) under visible light. The TiO_2 NTs were prepared by first prepared by the hydrothermal method and subsequently loaded with Cu/Ni metal nanoparticles by the impregnation reduction method. The structure, morphology, and chemical composition of the as-obtained catalysts were characterized by X-ray diffraction (XRD), scanning electron microscopy coupled with energy dispersive X-ray spectroscopy (SEM-EDX), transmission electron microscopy (TEM), inductively coupled plasma emission spectroscopy (ICP), and ultraviolet–visible spectroscopy (UV-Vis). The characterization results revealed that the metal nanoparticles were uniformly loaded on the surface of the TiO_2 NTs, while the band gap of the catalyst was reduced significantly from 3.22 to 2.68 eV. The catalysts showed an excellent photocatalytic performance towards the hydrolysis of AB for H_2 production. Thus, the H_2 production rate of $Cu_{0.64}Ni_{0.36}$-TiO_2 NTs reached 5763.86 mL g^{-1}·min^{-1}, with a total turnover frequency (TOF) of 15.90 mol H_2·(mol cat)$^{-1}$·min^{-1} for a loading volume of metal particles of 5.25 wt%. The results presented herein demonstrate that TiO_2(B) can be a potential photocatalyst for effective H_2 production, and also provide a cheap and effective approach to improve the light-to-H_2 energy conversion.

Introduction

In recent years, H_2 has become the most important energy vector owing to its high energy density, non-toxicity, and zero emission characteristics.[1, 2] Since H_2 storage requires high pressure and complex technology, a large number of new H_2 storage technologies and materials have been recently developed.[3, 4] Some H_2 storage materials including ammonia borane (NH_3BH_3, AB), sodium borohydride, decaborane, and formic acid have demonstrated large hydrogen storage capacities.[5-9] In particular, AB is non-toxic and combines high hydrogen content (19.6 wt%) and low molecular weight (30.7 g·mol^{-1}), making it the most attractive candidate material for hydrogen storage.[10, 11]

AB can be dehydrogenated by three different ways namely, thermal decomposition, alcoholysis, and hydrolysis. Among these methods, hydrolysis is particularly convenient and has been widely used.[12] AB can produce a certain amount of H_2 at room temperature via a catalytic reaction. In this sense, efficient catalysts are required to present high catalytic rate and a good stability. Although various noble metal (e.g., Au, Ag, Ru, and Pt, among others) nanoparticles have been used as catalysts in AB hydrogen storage applications, their high costs and limited availability have hindered wide applications.[13-17] In contrast, transition metals (e.g., Co, Ni, and Cu, among others) are cheaper and possess high catalytic efficiencies.[18-20] However, in order to prevent aggregation of the metal particles during the reaction process, it is imperative to find a feasible carrier material such as carbon NTs, metal organic frameworks, and graphene.[21-25] Yu prepared CuNi nanoparticles supported on graphene (G-$Cu_{36}Ni_{64}$ NPs) and used them for the catalytic release of H_2 from AB.[26] This catalyst showed an initial turnover frequency (TOF) of 49.1 mol_{H2} mol_{CuNi}^{-1} min^{-1} and an activation energy (*E*a) of 24.4 kJ mol^{-1}. Gao prepared Cu_2Ni_1@MIL-101 by in-situ reduction and liquid impregnation methods. The catalyst exhibited high catalytic activity a TOF of 20.9 mol H_2 min^{-1} Cu mol^{-1} and a very low *E*a of 32.2 kJ mol^{-1}.[27] However, these catalysts suffer from high cost for the support material and complex preparation processes.

An increasing number of works have been published recently on the use of TiO_2-based catalysts for the production of H_2 from AB. Kohsuke supported Ru−Ni nanoparticles on TiO_2 by impregnation and then reduction by H_2. The catalysts showed high activity, with a total TOF of 914 min^{-1} and an Ea of 28.1 kJ mol^{-1}.[11] Jo prepared a highly active Au/TiO_2 catalysts towards H_2 generation which produced 88 μmol of H_2 in 4 h.[28] Murat prepared a Co–P/TiO_2 catalyst by electrolysis deposition, and this material showed a H_2 generation rate of 2002 mL H_2 min^{-1} (g catalyst)$^{-1}$ and an *E*a of 48.1 kJ mol^{-1}.[29] Yousef prepared Cu-doped titania nanofibers by electrospinning. This material showed a H_2 equivalent of 2.7 after 10 min, and this value remained unchanged after three successive reaction cycles.[12] Single metals or the combination of transition metals and noble metals have been mostly supported on TiO_2. Previous reports on metal nanoparticles supported TiO_2 nanofibers have

[a] School of Materials Science and Engineering, Hebei University of Technology, Tianjin, 300130, PR China
* Corresponding authors

revealed a relatively single morphology for the support. The resultant composite material showed low catalytic activity towards the hydrolysis of AB. The high specific surface area of TiO_2 NTs provides these materials with improved light absorption and scattering properties and high adsorption capacity, making them good support materials for metal loading.[30] Supported bimetallic transition metals can result in synergies between the metals, which can significantly improve the catalytic activity and reduce the price of the catalyst.

In this work, TiO_2(B) NTs were first prepared by the hydrothermal method and subsequently loaded with Cu/Ni metal nanoparticles via a redox replacement reaction. The metal particles were uniformly distributed on the surface of the NTs and exhibited good photocatalytic catalytic activity towards the production of H_2 from AB.

Experimental

Preparation of TiO_2(B) NTs

For a typical hydrothermal synthesis of TiO_2(B) NTs, 0.1 g of TiO_2 (anatase, commercial) powder were dissolved in 25 mL of a NaOH solution (10 mol L^{-1}) and ultrasonically dispersed for 30 min. The mixed solution was transferred to a Teflon-lined stainless-steel autoclave and reacted at 160 ℃ for 8 h. After the hydrothermal reaction, the resultant product was centrifuged, washed with deionized water, and soaked in a 0.1 M HCl solution overnight. The precipitate was washed several times with water and ethanol, and dried at 80 ℃ overnight. Finally, the resultant white powder was calcined in air at 400 ℃ for 6 h to obtain TiO_2(B) NTs.

Preparation of Cu_x/Ni_{1-x} -TiO_2(B) NTs

The Cu_x/Ni_{1-x} supported TiO_2(B) NT materials were synthesized by a chemical reduction method. The metal-ion precursors ($M(NO_3)_2$, M = Cu and Ni) were dissolved in 24 mL of water, and an ammonia solution was added drop by drop to form a clear solution. Then, 0.2 g of the as-prepared TiO_2(B) NTs powder was added to the solution and stirred for 24 h to form a suspension. The precipitate was collected by centrifugation and washed with 15 mL of water in a round bottom flask. A 0.6 M $NaBH_4$ solution was added to the dispersed solution to reduce metal ions under an ice-water bath. After 1 h of reaction, the resultant product was recovered by centrifugation, washed three times with water, and freeze-dry overnight to finally obtain Cu_x/Ni_{1-x} supported TiO_2(B) NTs.

Catalysts characterization

The as-synthesized catalysts were characterized by powder X-ray diffraction (XRD, Rigaku D/max-2500 X-ray generator, Cu Ka radiation), scanning electron microscopy coupled with energy dispersive X-ray spectroscopy (SEM-EDX, JEOL JSM-6700F), transmission electron microscopy (TEM, Philips Tecnai F20, 200 kV), inductively coupled plasma emission spectroscopy (ICP), UV-vis spectrophotometry (UV-vis, Hitachi U-3900H), and X-ray photoelectron spectroscopy (XPS).

H_2 generation measurements

H_2 production experiments were carried out in a photocatalytic reactor with a volumetric capacity of 100 mL. A Xe lamp placed on the top of the photoreactor was used as the light source for the H_2 production reaction. The reaction solution in the photoreactor contained 0.0260 g of catalyst and 10 mL of a 0.5 wt% AB solution. The reaction device was subjected to a hydrolysis reaction under magnetic stirring in a temperature-controlled bath. The volume of H_2 released was measured by a micro-gas flowmeter (RTK-GMA-Ⅱ). The hydrolysis of AB can be described as follows:[31]

$$NH_3BH_3 + 2H_2O \rightarrow NH_4^+{}_{(aq)} + BO_2^-{}_{(aq)} + 3H_{2(g)} \quad (1)$$

The catalytic properties of the Cu_x/Ni_{1-x}-TiO_2(B) NT composites towards the production of H_2 were compared under visible light, UV light, and darkroom conditions.

Results and discussion

Catalyst characterization

In this study, TiO_2 nanotubes support was prepared by hydrothermal method. The hydrothermal reaction using concentrated NaOH as solvent can change the morphology of raw materials and form NTs under appropriate temperature and time conditions. The product was washed with water and soaked in HCl solution, in which Na^+ was replaced by H^+, and then calcined to form TiO_2 nanotubes. The TiO_2 NTs is immersed in the metal ammonia complex ion solution so that the metal ions can be uniformly adsorbed on the surface of the support. Centrifugation to remove excess unabsorbed metal ions. Excessive amount of $NaBH_4$ reduced the metal ions that adsorbed on the surface of the support. Since the reducing agent will generate H_2 during the reaction that can a protective gas to prevent metal particles from oxidation. Thus, pure

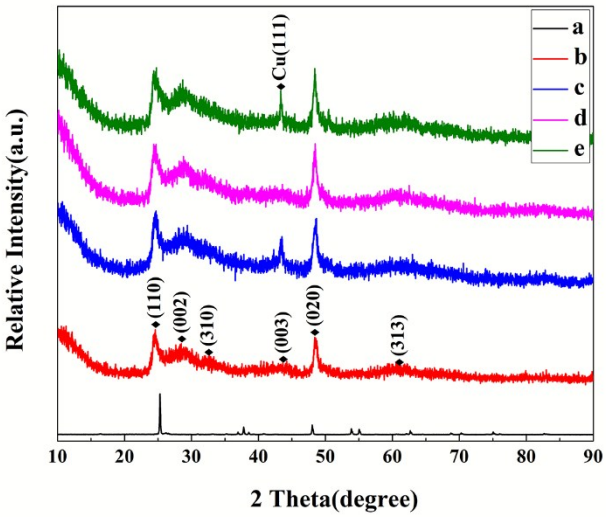

Fig. 1-XRD patterns of TiO_2 nanoparticles (a), TiO_2(B) NTs (b), Cu-TiO_2(B) NTs (c), Ni-TiO_2(B) NTs (d), and $Cu_{0.64}Ni_{0.36}$-TiO_2(B) NTs (e).

catalysts with high activity can be prepared.

As shown in Fig. 1a, the XRD pattern of commercial TiO_2 nanoparticles revealed the presence of an anatase phase before

View Article Online
DOI: 10.1039/C8QI00492G

the hydrothermal reaction (JCPDS file 21-1272). After reaction and calcination, the XRD diffraction peaks of TiO_2(B) NTs revealed the presence of a beta-TiO_2 phase (JCPDS file 46-1237) with peaks at 2θ of 24.9, 28.6, and 48.5°, which can be indexed to the (110), (002), and (020) crystal planes of beta-TiO_2 (Fig. 1b). After loading metal nanoparticles (Figs. 1c–e), a diffraction peak corresponding to a Cu crystal phase (2θ = 43.3°) appeared, demonstrating that Cu nanoparticles were actually loaded. However, no significant diffraction peaks were observed for Ni, which can be explained by the amorphous nature of Ni nanoparticles producing weak diffraction peaks, as was the case for $Cu_{0.64}Ni_{0.36}$-TiO_2(B) NTs.

Table 1-The ratios of Cu/Ni for Cu_xNi_{1-x} tested by ICP

Samples	Cu	$Cu_{0.75}Ni_{0.25}$	$Cu_{0.67}Ni_{0.33}$	$Cu_{0.5}Ni_{0.5}$	$Cu_{0.25}Ni_{0.75}$	$Cu_{0.17}Ni_{0.83}$	Ni
Cu:Ni(mol%)	-	0.82:0.18	0.76:0.24	0.64:0.36	0.46:0.54	0.32:0.68	-
(Cu+Ni):(Cu+Ni+TiO_2)(wt%)	0.0954	0.0473	0.0516	0.0525	0.0448	0.0458	0.0429

Fig. 2 shows SEM and TEM images of the unloaded TiO_2(B) NTs and the TiO_2(B) NTs loaded with metal nanoparticles. Comparing the morphology, the surface of the unloaded TiO_2(B) NTs was relatively smooth, with NTs of 10–40 nm and several micrometres in diameter and in length, respectively, and with a high aspect ratio (Fig. 2a). The catalyst loaded with nano-metal particles showed a rough surface, and the protuberances produced by the nanoparticles were clearly observed. The nanoparticles were small and evenly dispersed on the surface of the NTs (Fig. 2b). Fig. 2c and 2d display typical TEM images of the unloaded TiO_2(B) NTs and $Cu_{0.64}Ni_{0.36}$-TiO_2(B) NTs. After loading with metal nanoparticles, the surface of the NTs revealed well-dispersed small black spots, which can be considered as metal particles. The NTs were further studied by high-resolution TEM (HRTEM). This technique revealed lattice fringes with interlayer spaces of 0.364 and 0.624 nm, which were ascribed to the (110) and (001) planes of TiO_2(B), respectively. The small black spots circled in red are considered to be uniformly loaded metal particles on the surface of the nanotubes with sizes of 0.8-1.8 nm. Element mapping test was performed to study the loading of metal elements on the carrier (Fig. 3a). As shown in Fig. 3a, Cu and Ni were uniformly distributed. EDX analysis revealed the presence of Cu and Ni, in addition to the TiO2(B) support (Fig. 3b).

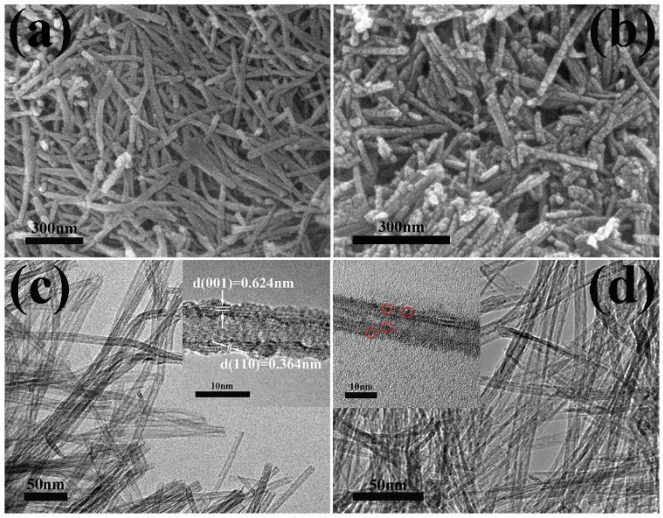

Fig. 2-SEM images of unloaded TiO_2(B) NTs (a), and $Cu_{0.64}Ni_{0.36}$-TiO_2(B) NTs (b). TEM image of unloaded TiO_2(B) NTs (c), and $Cu_{0.64}Ni_{0.36}$-TiO_2(B) NTs (d).

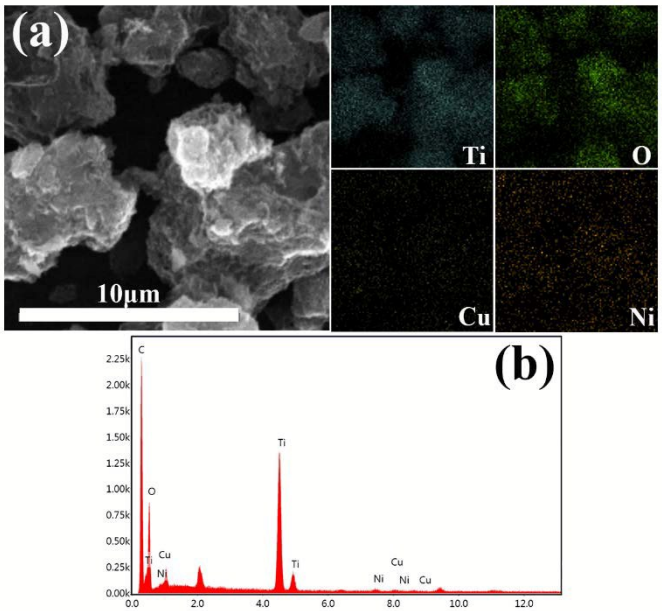

Fig. 3-The Ti, O, Cu, Ni elemental mapping of $Cu_{0.64}Ni_{0.36}$-TiO_2(B) NTs(a). The EDS spectra of $Cu_{0.64}Ni_{0.36}$-TiO_2(B) NTs (b).

Different Cu_xNi_{1-x}-TiO_2(B) NT materials (x = 1, 0.75, 0.67, 0.5, 0.25, 0.17, and 0, with x being the raw material ratio) were prepared by changing the ratio of Cu and Ni during the preparation. The elemental composition of the prepared Cu_xNi_{1-x}-TiO_2(B) NT samples was determined by ICP elemental analysis. The specific metal ratios and loaded amounts are listed in Table 1.

The photocatalytic activity of semiconductors is closely related to their forbidden band width. Fig. 4 shows the UV absorption spectra of pure TiO_2(B) NTs and TiO_2(B) NTs loaded with Cu, Ni,

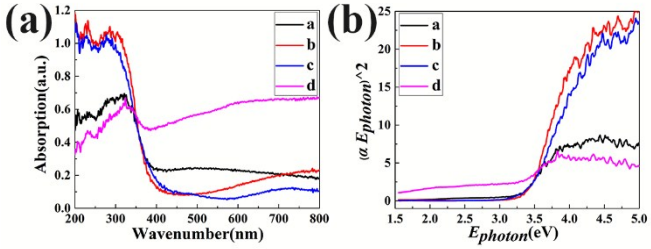

Fig. 4-UV-Vis spectra of TiO_2(B) NTs (a), Cu-TiO_2(B) NTs (b), Ni-TiO_2(B) NTs (c), and $Cu_{0.64}Ni_{0.36}$-TiO_2(B) NTs (d) (a) and the plot of $(\alpha h\nu)^2$ versus hv curve to estimate the band gap energy (b).

View Article Online
DOI: 10.1039/C8QI00492G

and Cu/Ni metal particles. As shown in Fig. 4, the absorption band edge of the spectrum shifted to the longer wavenumbers upon loading of the metal nanoparticles, being gradually red-shifted until reaching the visible light region. The absorption coefficient (α) and the semiconductor band gap (E_g) are related with the following expression:

$(\alpha h\nu)^2 \propto h\nu - E_g$

where ν stands for the frequency and h is the Planck´s constant. Fig. 4b represents the relationship between $(\alpha h\nu)^2$ and hν. As estimated by the tangent intercept of the curve, the band gap energies of TiO_2(B) NTs, Cu-TiO_2(B) NTs, Ni-TiO_2(B) NTs, $Cu_{0.64}Ni_{0.36}$-TiO_2(B) NTs were 3.22, 3.20, 3.16, and 2.68 eV, respectively. These results indicated that the loading of the Cu/Ni metal particles significantly enhanced the light absorption region, reducing the bandgap of the catalyst and therefore increasing the catalytic performance of the photocatalyst.

In order to determine the composition and chemical state of the supported metal elements, the surface of the materials was characterized by XPS. The XPS spectrum of $Cu_{0.64}Ni_{0.36}$-TiO_2(B) NTs contained several peaks, and their fittings are shown in Fig. 5. As shown in Fig. 5a, fitting of the Cu2p band revealed two peaks at 932.6 and 952.2 eV, which were ascribed to Cu(0)2p3/2 and Cu(0)2p1/2 transitions, respectively. The presence of metal Cu(0) was demonstrated. The fitting of the Ni2p peak (Fig. 5b) revealed six peaks: 852.6 eV corresponding to Ni(0)2p3/2, 855.9 eV corresponding to Ni(II)2p3/2, 869.7 eV corresponding to Ni(0)2p1/2, and 873.7 eV corresponding to Ni(II)2p1/2. In addition, Ni(II)2p3/2 and Ni(II)2p1/2 satellite peaks were observed at 861.7 and 880.0eV, respectively, indicating the presence of metallic nickel and Ni^{2+} species. This result showed that metallic Cu was stable in the catalyst, while metallic Ni was partially oxidized. Since the redox potentials of Cu^{2+} and Ni^{2+} are 0.342 and -0.257 V, respectively, Cu^{2+} are likely to be reduced first during the reduction step of the reduction process.[32] In a subsequent step, Ni^{2+} can be reduced to generate a Ni shell on the surface of the Cu core, resulting in the final Cu@Ni structure.[33] The surface of Ni metal is readily oxidized, and, once formed, this oxidation shell protects Cu metal from oxidation. Since the sample was exposed to air during the XPS test, the oxidation state of Ni was present. we think that nickel oxide is not the active site of the catalytic reaction. Nickel oxide has no catalytic activity for ammonia borane by itself. The XPS of Ni@h-BN prepared by Wu[34] and CuNi-MIL-101 prepared by Gao[27] both showed the existence of metal oxidation state, but it did not participate in the catalytic reaction as active sites.

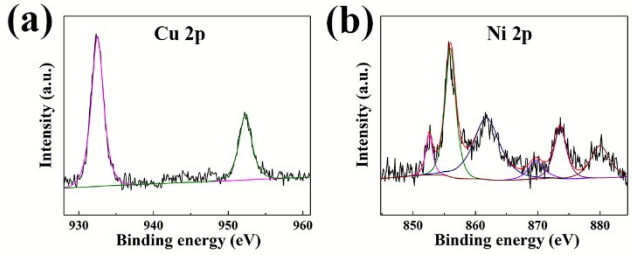

Fig. 5- XPS spectra of $Cu_{0.64}Ni_{0.36}$-TiO_2(B) NTs: Cu2p (a) and Ni2p (b).

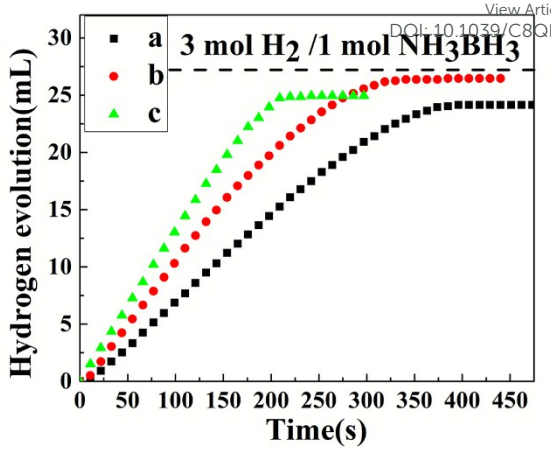

Fig. 6-Hydrogen generation from AB (0.5 wt %, 10 mL) containing as-prepared catalysts (0.0260g) at 25 °C with different conditions: visible light (a), UV light (b), darkroom (c)

Catalytic activities

Fig. 6 shows the amount of H_2 as a function of time for the 5.25 wt% $Cu_{0.64}Ni_{0.36}$-TiO_2(B) NTs sample under visible light, UV light, and darkroom conditions. Under visible light conditions, the H_2 production reached 5763.86 mL g^{-1}·min^{-1}, with a TOF of 15.90 mol H_2· (mol cat)$^{-1}$·min^{-1}. This value was higher than those obtained under UV (4598.69 mL g^{-1}·min^{-1}) and darkroom (3419.77 mL g^{-1}·min^{-1}) conditions. Therefore, it can be concluded that the light absorption region of the composite was widened reaching the visible region as a result of the loading of metal particles. The catalytic activity of the catalyst increased as a result of the enhanced light absorption and the reduced band gap. Therefore, the photocatalytic AB H_2 production method developed herein can be efficiently carried out under visible light conditions. Regarding the H_2 production rate, the catalyst developed herein showed significantly higher values than the Cu/Co catalyst (ca.1000 mL (min^{-1} g_{cat})) reported by Li et al,[35] and the $Cu_{0.2}Ni_{0.8}$/MCM-41 system (10.7 mol H_2 mol $catalyst^{-1}$ min^{-1}) reported by Lu et al.[36]

Fig. 7a shows the H_2 content as a function of time during the hydrolysis of of AB over Cu_xNi_{1-x}-TiO_2(B) NTs. The unloaded pure TiO_2(B) NTs did not show any catalytic activity (curve a), while the monometallic supported TiO_2(B) NT samples (Cu-TiO_2(B) NTs and Ni-TiO_2(B) NTs) showed low catalytic activity (curves b and h). The H_2 production rate of the bimetallic catalyst Cu_xNi_{1-x}-TiO_2(B) NTs was higher than the rest of the samples. The H_2 generation rates after addition of Cu and Ni are summarized in Table 2. Although the nominal ratio of Cu and Ni during the preparation was 1:1, the actual metal ratio of $Cu_{0.64}Ni_{0.36}$ was determined by ICP, and the metal loading was 5.25 wt%. The

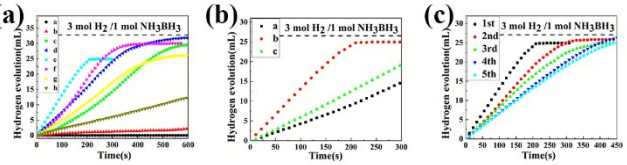

Fig. 7-Hydrogen generation from AB (0.5 wt%, 10 mL) containing as-prepared catalysts Cu_xNi_{1-x}-TiO_2(B) NTs (0.0260g) under visible light. (a) Different Cu content in Cu_xNi_{1-x}-TiO_2(B) NTs: pure TiO2(B) NTs (a), x=1 (b), x=0.82 (c), x=0.76 (d), x=0.64 (e), x=0.46 (f), x=0.32 (g), x=0 (h); (b) Varying Cu/Ni loadings: 3.97% (a), 5.25% (b), 6.37% (c); (c) Cycling performance of the prepared $Cu_{0.64}Ni_{0.36}$-TiO_2(B) NTs (5.25 wt%) catalyst.

View Article Online
DOI: 10.1039/C8QI00492C

$Cu_{0.64}Ni_{0.36}$-TiO_2(B) NTs catalyst showed optimum catalytic performance, with a H_2 production rate as high as 5763.86 mL g^{-1}·min^{-1} and TOF of 15.90 mol H_2·(mol cat)$^{-1}$·min^{-1}. This value was significantly larger than that of a Cu catalysts supported on reduced graphene oxide (Cu/RGO, 3.61 mol H_2 mol per catalyst per min)[24] and also significantly higher than that of Co–B nanoflakes-TiO_2 nanofibers (ca. 2745.6 mL g^{-1}·min^{-1}).[37] The higher catalytic activity of the bimetallic material revealed that bimetallic loading can result in higher catalytic efficiencies over single metal. The catalytic properties of several catalysts are summarized in Table 3. Compared with other catalysts, the TOF of the catalyst developed herein (15.90 mol H_2·(mol cat)$^{-1}$·min^{-1}) is higher than other non-noble catalysts, but slightly lower than that of catalysts containing noble metals.

Table 2-Hydrogen generation rate for the prepared Cu_xNi_{1-x} -TiO_2(B) NTs catalysts

Catalyst	Slope of the fitting line (mL·min^{-1})	H_2 generation ratio (mL·min^{-1}·g^{-1})	TOF (mol H_2·(mol cat)$^{-1}$·min^{-1})
Cu-TiO_2(B) NTs	0.4000	161.116	0.4571
$Cu_{0.82}Ni_{0.18}$-TiO_2(B) NTs	4.280	3477.13	9.729
$Cu_{0.76}Ni_{0.24}$-TiO_2(B) NTs	4.843	3607.34	10.05
$Cu_{0.64}Ni_{0.36}$-TiO_2(B) NTs	7.873	5763.86	15.90
$Cu_{0.46}Ni_{0.54}$-TiO_2(B) NTs	5.896	5066.75	13.78
$Cu_{0.32}Ni_{0.68}$-TiO_2(B) NTs	3.750	3149.04	8.467
Ni-TiO_2(B) NTs	1.517	1359.63	3.562

The influence of the metal particle loading on the photocatalytic performance followed a volcano-type behavior. Thus, $Cu_{0.64}Ni_{0.36}$-TiO_2(B) NTs showed the highest catalytic activity for a Cu/Ni loading of 5.25 wt% (Fig. 7b). This catalyst showed higher H_2 generation rates (5763.86 mL g^{-1}·min^{-1}) than the catalysts with a Cu/Ni loading of 3.97 wt% (2925.01 mL g^{-1}·min^{-1}) and 6.37 wt% (2281.98 mL g^{-1}·min^{-1}). A proper loading content is beneficial to the interaction between the active sites and the carrier material. In addition, the aggregation produced when the metal particles act directly as a catalyst can be suppressed. In order to investigate the cycle performance and durability of the catalyst developed herein, $Cu_{0.64}Ni_{0.36}$-TiO_2(B) NTs was tested five times. As shown in Fig. 7c, although the catalyst showed excellent performance during the first reaction cycle, the H_2 production rate decreased slightly with the number of cycles. Thus, the catalysts preserved 49% of the original H_2 production rate after five reaction cycles. In order to illustrate the change of the $Cu_{0.64}Ni_{0.36}$-TiO_2(B) NTs after the first hydrogenation of AB, the SEM and TEM images are shown in Fig 8. From the SEM image (Fig. 8a), it can be seen that the tubular morphology of the catalyst is less obvious, and more NTs collapse and expand. The appearance is not uniform before the catalytic reaction. Also, in the TEM image (Fig. 8b), the cracked film of the nanotubes can be clearly seen in the red line. The change in morphology after the catalytic reaction may result in a significant reduction in the performance of the catalyst. In addition, we hypothesized that the metal particles were progressively oxidized to a certain extent as the number of cycles increased, affecting negatively to the catalytic efficiency.

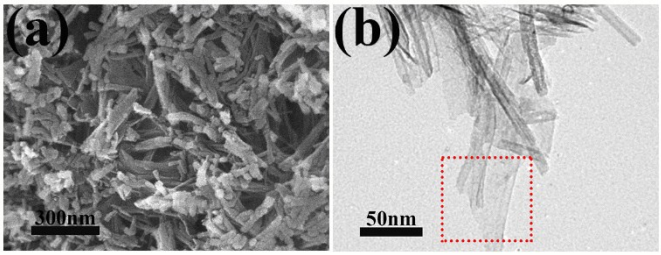

Fig. 8-SEM(a) and TEM(b) images of $Cu_{0.64}Ni_{0.36}$-TiO_2(B) NTs that completed catalytic reaction for once

Table 3-Catalytic activity of catalysts used for the hydrolytic dehydrogenation of AB.

Catalyst	H_2 generation ratio (mL·min^{-1}·g^{-1})	TOF (mol H_2·(mol cat)$^{-1}$·min^{-1})	Ea(kJ/mol^{-1})	Ref.
RGO-$Cu_{75}Pd_{25}$	-	26.6	45 ± 3	38
$Ni_{0.33}$@$Pt_{0.67}$/C	5469	-	33.0	39
Pd NPs/CS	-	24.96	36.25	40
CuNi-MIL-101	-	20.9(Cu)	32.2	27
Cu/RGO	-	3.61	38.2±1.5	24
Cu@SiO_2	-	3.24	36±1	41
$Ni_{91}P_9$/rGO	-	13.3	34.7	42
Co^0/CeO_2	-	7.0	43±2	43
Co–P/TiO_2	2002	-	48.1	29
P(AMPS)-Co	2921	-	47.7	44
Ni/BN	476.1	1.03	61.1	45
$Ni_{0.19}Cu_{0.81}$	2066	2.7	33.3	19
$Cu_{0.2}Ni_{0.8}$/MCM-41	-	10.7	38	36
CuCo/graphene	-	9.81	-	46
CuNi@Carbon	-	0.2	28.9	47
Cu@FeCo	-	10.5	38.75	48
Cu@FeNi	-	8.37	32.9	49
$Cu_{0.2}Co_{0.8}$/HPC	2960	-	41.7	50
$Cu_{0.64}Ni_{0.36}$-TiO_2(B) NTs	5763.86	15.9	36.14	this work

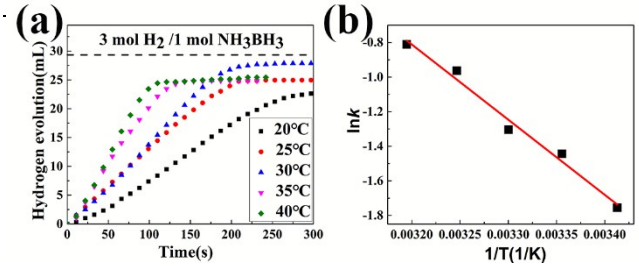

Fig. 9-Effect of temperature on the hydrogen generation rate using 0.0260 g of 5.25wt% $Cu_{0.64}Ni_{0.36}$-TiO_2(B) NTs in AB solution (0.5 wt %, 10 mL) at atmospheric pressure (a), and Arrhenius plots of ln *k* vs the reciprocal absolute temperature 1/T (b).

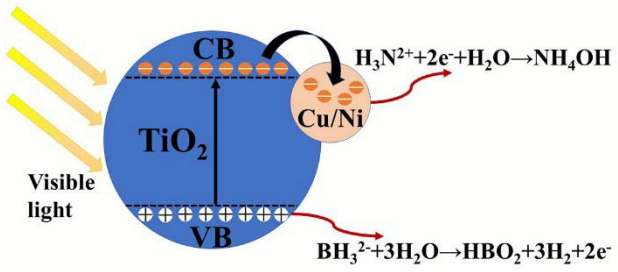

Fig. 10-Mechanism of photocatalytic hydrolysis of ammonia borane over Cu/Ni-TiO_2 NTs under visible light irradiation.

Fig. 9a shows the amount of H_2 released via hydrolysis of AB over $Cu_{0.64}Ni_{0.36}$-TiO_2(B) NTs at different temperatures. As shown in Fig. 9, the H_2 release rate increased with temperature. Fig. 9b shows the Arrhenius plots (i.e., lnk versus the reciprocal absolute temperature (1/T)) for the catalyst under study. By fitting the points to a straight line, the correlation coefficient in the resulting straight line fitting result is -0.9924. According to the slopes of the straight sections, the apparent Ea of the catalyst was 36.14 kJ mol^{-1}. This value was lower than that previously reported (38 kJ·mol^{-1}) for $Cu_{0.2}Ni_{0.8}$/MCM-41[36] and Cu@Ni[51] (40.53 kJ/mol) catalysts.

In order to describe the photocatalytic AB hydrolysis mechanism of the catalyst prepared in this paper, we described the energy band structure and the separation of electron–hole pairs inside the catalyst (Fig. 10). Considering the entire catalytic system, the support TiO_2 generates photogenerated electrons and holes when irradiated with visible light. New electron trapping sites can be formed after the loading of metals on the surface of TiO_2. Photogenerated electrons can be transferred from the conduction band of TiO_2 to the metal nanoparticles. The ability of the metal particles to trap electrons is improved as a result of the formation of a Schottky barrier between the metal nanoparticles and TiO_2.[52,53] The photoelectrons and holes are therefore separated effectively, and the photocatalytic activity of the catalyst improves significantly as a result.

Conclusions

In summary, we prepared TiO_2(B) NTs-supported Cu/Ni metal nanoparticles by the hydrothermal and impregnation–reduction methods. The characterization results revealed that the light absorption region of the composite material expanded to the visible light region and the bandgap of the material decreased. As a result, the recombination rate of photogenerated electrons and holes was significantly reduced, improving the photocatalytic performance of the material. The catalyst exhibited higher catalytic rates and lower Ea for the photocatalytic hydrolysis of AB. Therefore, we provided herein a low-cost and simple-preparation material with good catalytic performance towards the hydrolysis of AB.

Conflicts of interest

There are no conflicts to declare.

Acknowledgements

View Article Online
DOI: 10.1039/C8QI00492G

This work was supported by the key Basic Research Programme of Hebei Province of China (17964401D), the National Natural Science Foundation of China (No. 21603052, 51771068 and 51771067), and the Natural Science Foundation of Hebei Province (No. B201820167).

References

1. T. da Silva Veras, T. S. Mozer, D. da Costa Rubim Messeder dos Santos and A. da Silva César, *International Journal of Hydrogen Energy*, 2017, **42**, 2018-2033.
2. S. E. Hosseini and M. A. Wahid, *Renewable and Sustainable Energy Reviews*, 2016, **57**, 850-866.
3. Q.-L. Zhu and Q. Xu, *Energy & Environmental Science*, 2015, **8**, 478-512.
4. S. Niaz, T. Manzoor and A. H. Pandith, *Renewable and Sustainable Energy Reviews*, 2015, **50**, 457-469.
5. P. Brack, S. E. Dann and K. G. U. Wijayantha, *Energy Science & Engineering*, 2015, **3**, 174-188.
6. D. Mellmann, P. Sponholz, H. Junge and M. Beller, *Chemical Society reviews*, 2016, **45**, 3954-3988.
7. R. Moury and U. Demirci, *Energies*, 2015, **8**, 3118-3141.
8. P.-Y. Olu, N. Job and M. Chatenet, *Journal of Power Sources*, 2016, **327**, 235-257.
9. A. Rossin and M. Peruzzini, *Chemical reviews*, 2016, **116**, 8848-8872.
10. M. O. Talbot, T. N. Pham, M. A. Guino-o, I. A. Guzei, A. I. Vinokur and V. G. Young, *Polyhedron*, 2016, **114**, 415-421.
11. K. Mori, K. Miyawaki and H. Yamashita, *ACS Catalysis*, 2016, **6**, 3128-3135.
12. A. Yousef, N. A. M. Barakat and H. Y. Kim, *Applied Catalysis A: General*, 2013, **467**, 98-106.
13. N. Blaquiere, S. Diallo-Garcia, S. I. Gorelsky, D. A. Black and K. Fagnou, *Journal of the American Chemical Society*, 2008, **130**, 14034-+.
14. J.-M. Yan, X.-B. Zhang, T. Akita, M. Haruta and Q. Xu, *Journal of the American Chemical Society*, 2010, **132**, 5326-+.
15. M. Chandra and Q. Xu, *Journal of Power Sources*, 2007, **168**, 135-142.
16. L. Yang, W. Luo and G. Cheng, *ACS applied materials & interfaces*, 2013, **5**, 8231-8240.
17. C. Yao, L. Zhuang, Y. Cao, X. Ai and H. Yang, *International Journal of Hydrogen Energy*, 2008, **33**, 2462-2467.
18. N. A. M. Barakat, M. Motlak, A. Taha, M. M. Nassar, M. S. Mahmoud and H. Fouad, *International Journal of Green Energy*, 2015, **13**, 642-649.
19. W. Sang, C. Wang, X. Zhang, X. Yu, C. Yu, J. Zhao, X. Wang, X. Yang and L. Li, *International Journal of Hydrogen Energy*, 2017, **42**, 30691-30703.
20. Q. Xu and M. Chandra, *Journal of Power Sources*, 2006, **163**, 364-370.
21. W. Chen, X. Duan, G. Qian, D. Chen and X. Zhou, *Chemsuschem*, 2016, **9**, 3019-3019.
22. N. Cao, T. Liu, J. Su, X. Wu, W. Luo and G. Cheng, *New Journal of Chemistry*, 2014, **38**, 4032.
23. X. Meng, L. Yang, N. Cao, C. Du, K. Hu, J. Su, W. Luo and G. Cheng, *ChemPlusChem*, 2014, **79**, 325-332.

24. Y. Yang, Z.-H. Lu, Y. Hu, Z. Zhang, W. Shi, X. Chen and T. Wang, *RSC Adv.*, 2014, **4**, 13749-13752.
25. J. Shen, N. Cao, Y. Liu, M. He, K. Hu, W. Luo and G. Cheng, *Catalysis Communications*, 2015, **59**, 14-20.
26. C. Yu, J. Fu, M. Muzzio, T. Shen, D. Su, J. Zhu and S. Sun, *Chemistry of Materials*, 2017, **29**, 1413-1418.
27. D. Gao, Y. Zhang, L. Zhou and K. Yang, *Applied Surface Science*, 2018, **427**, 114-122.
28. S. Jo, P. Verma, Y. Kuwahara, K. Mori, W. Choi and H. Yamashita, *J. Mater. Chem. A*, 2017, **5**, 21883-21892.
29. M. Rakap, *Journal of Power Sources*, 2014, **265**, 50-56.
30. F. X. Xiao, J. Miao, H. B. Tao, S. F. Hung, H. Y. Wang, H. B. Yang, J. Chen, R. Chen and B. Liu, *Small*, 2015, **11**, 2115-2131.
31. M. Rakap, *Journal of Alloys and Compounds*, 2015, **649**, 1025-1030.
32. T. Yamauchi, Y. Tsukahara, T. Sakata, H. Mori, T. Yanagida, T. Kawai and Y. Wada, *Nanoscale*, 2010, **2**, 515-523.
33. J.-H. Lin and V. V. Guliants, *Applied Catalysis A: General*, 2012, **445-446**, 187-194.
34. Y. Wu, X. Wu, Q. Liu, C. Huang and X. Qiu, *International Journal of Hydrogen Energy*, 2017, **42**, 16003-16011.
35. C. Li, J. Zhou, W. Gao, J. Zhao, J. Liu, Y. Zhao, M. Wei, D. G. Evans and X. Duan, *Journal of Materials Chemistry A*, 2013, **1**.
36. Z.-H. Lu, J. Li, G. Feng, Q. Yao, F. Zhang, R. Zhou, D. Tao, X. Chen and Z. Yu, *International Journal of Hydrogen Energy*, 2014, **39**, 13389-13395.
37. A. Yousef, R. M. Brooks, M. M. El-Halwany, M. Obaid, M. H. El-Newehy, S. S. Al-Deyab and N. A. M. Barakat, *International Journal of Hydrogen Energy*, 2016, **41**, 285-293.
38. K. Güngörmez and Ö. Metin, *Applied Catalysis A: General*, 2015, **494**, 22-28.
39. X. Yang, F. Cheng, J. Liang, Z. Tao and J. Chen, *International Journal of Hydrogen Energy*, 2011, **36**, 1984-1990.
40. X. Chen, X.-J. Xu, X.-C. Zheng, X.-X. Guan and P. Liu, *Materials Research Bulletin*, 2018, **103**, 89-95.
41. Q. Yao, Z.-H. Lu, Z. Zhang, X. Chen and Y. Lan, *Scientific Reports*, 2014, **4**.
42. X. Du, C. Yang, X. Zeng, T. Wu, Y. Zhou, P. Cai, G. Cheng and W. Luo, *International Journal of Hydrogen Energy*, 2017, **42**, 14181-14187.
43. S. Akbayrak, O. Taneroğlu and S. Özkar, *New Journal of Chemistry*, 2017, **41**, 6546-6552.
44. O. Ozay, E. Inger, N. Aktas and N. Sahiner, *International Journal of Hydrogen Energy*, 2011, **36**, 8209-8216.
45. X. J. Yang, L. L. Li, W. L. Sang, J. L. Zhao, X. X. Wang, C. Yu, X. H. Zhang and C. C. Tang, *Journal of Alloys and Compounds*, 2017, **693**, 642-649.
46. J.-M. Yan, Z.-L. Wang, H.-L. Wang and Q. Jiang, *Journal of Materials Chemistry*, 2012, **22**.
47. A. Yousef, N. A. M. Barakat, M. El-Newehy and H. Y. Kim, *International Journal of Hydrogen Energy*, 2012, **37**, 17715-17723.
48. F. Qiu, Y. Dai, L. Li, C. Xu, Y. Huang, C. Chen, Y. Wang, L. Jiao and H. Yuan, *International Journal of Hydrogen Energy*, 2014, **39**, 436-441.
49. H.-L. Wang, J.-M. Yan, Z.-L. Wang and Q. Jiang, *International Journal of Hydrogen Energy*, 2012, **37**, 10229-10235.
50. H. Wang, L. Zhou, M. Han, Z. Tao, F. Cheng and J. Chen, *Journal of Alloys and Compounds*, 2015, **651**, 382-388.
51. J. Zhang, H. Li, H. Zhang, Y. Zhu and G. Mi, *Renewable Energy*, 2016, **99**, 1038-1045.
52. Z. Li, J. Liu, D. Wang, Y. Gao and J. Shen, *International Journal of Hydrogen Energy*, 2012, **37**, 6431-6437.
53. X. Fan, J. Fan, X. Hu, E. Liu, L. Kang, C. Tang, Y. Ma, H. Wu and Y. Li, *Ceramics International*, 2014, **40**, 15907-15917.